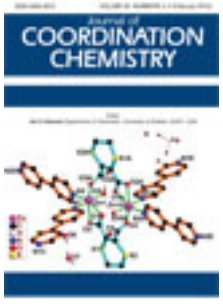

Journal of Coordination Chemistry
Publication details, including instructions for authors and subscription information:
http://www.tandfonline.com/loi/gcoo20

Synthesis, characterization, and thermodynamic studies of the interaction of some new water-soluble Schiff-base complexes with bovine serum albumin

Mozaffar Asadi [a], Somaye Barzegar Sadi [a], Zahra Asadi [a], Reza Yousefi [b], Ahmad Reza Barzegar Sadi [c] & Hojjat Khalili-Hezarjaribi [b]

[a] Chemistry Department, College of Sciences, Shiraz University, Shiraz 71454, I.R. Iran
[b] Biology Department, College of Sciences, Shiraz University, Shiraz 71454, I.R. Iran
[c] Department of Chemical Engineering, Iran University of Science and Technology, Tehran 16846, Iran
Published online: 14 Feb 2012.

To cite this article: Mozaffar Asadi, Somaye Barzegar Sadi, Zahra Asadi, Reza Yousefi, Ahmad Reza Barzegar Sadi & Hojjat Khalili-Hezarjaribi (2012) Synthesis, characterization, and thermodynamic studies of the interaction of some new water-soluble Schiff-base complexes with bovine serum albumin, Journal of Coordination Chemistry, 65:4, 722-739, DOI: 10.1080/00958972.2012.661419

To link to this article: http://dx.doi.org/10.1080/00958972.2012.661419

Journal of Coordination Chemistry
Vol. 65, No. 4, 20 February 2012, 722–739

Synthesis, characterization, and thermodynamic studies of the interaction of some new water-soluble Schiff-base complexes with bovine serum albumin

MOZAFFAR ASADI*†, SOMAYE BARZEGAR SADI†, ZAHRA ASADI†, REZA YOUSEFI‡, AHMAD REZA BARZEGAR SADI§ and HOJJAT KHALILI-HEZARJARIBI‡

†Chemistry Department, College of Sciences, Shiraz University, Shiraz 71454, I.R. Iran
‡Biology Department, College of Sciences, Shiraz University, Shiraz 71454, I.R. Iran
§Department of Chemical Engineering,
Iran University of Science and Technology, Tehran 16846, Iran

(*Received 29 October 2011; in final form 19 December 2011*)

Some new water-soluble Schiff-base complexes $Na_2[M(5\text{-}SO_3\text{-}2,3\text{-salpyr})(H_2O)_n]\cdot 2H_2O$ (5-SO_3-2,3-salpyr = *N*,*N*′-bis(5-sulphosalicyliden)-2,3-diaminopyridine and M = Zn, Cu, Ni) were synthesized and characterized by elemental analysis, IR, ^{1}H NMR, magnetic susceptibility measurement, thermal analysis, and UV-Vis spectroscopy. The mechanism of binding of $Na_2[M(5\text{-}SO_3\text{-}2,3\text{-salpyr})(H_2O)_n]\cdot 2H_2O$ with bovine serum albumin (BSA) was investigated by fluorescence spectroscopy. The fluorescence titration revealed that the intrinsic fluorescence of BSA was quenched by $Na_2[M(5\text{-}SO_3\text{-}2,3\text{-salpyr})]$, which was rationalized in terms of the static quenching mechanism. The values of the Stern–Volmer constants, quenching rate constants, binding constants, binding sites, and average aggregation number of BSA were determined by this method. Thermodynamic parameters were calculated by the van't Hoff equation. The data clearly indicate that the binding is entropy driven and enthalpically disfavored. Based on the Förster theory of non-radiative energy transfer, the efficiency of energy transfer, and the distance between the donor (Trp residues) and the acceptor ($Na_2[M(5\text{-}SO_3\text{-}2,3\text{-salpyr})]$) were evaluated. Also the synchronous fluorescence spectra showed that the microenvironment of the tryptophan residues was not changed. Finally, our results indicate that the complexes can bind to BSA and be efficiently transported in the body, which could be helpful for further drug design.

Keywords: Schiff base; Bovine serum albumin; Fluorescence

1. Introduction

Schiff-base complexes are an important class of compounds in medicinal and pharmaceutical development, with applications including excellent antibacterial [1–7], antifungal [3–5], and anticancer properties [6–10]. Diamino tetradentate Schiff bases and their complexes have been used as biological models in understanding the structure of biomolecules and biological processes [11, 12]. Study of interaction of metal

*Corresponding author. Email: asadi@susc.ac.ir

ISSN 0095-8972 print/ISSN 1029-0389 online
http://dx.doi.org/10.1080/00958972.2012.661419

complexes containing N_2O_2 Schiff-base ligands in biological systems has been published in a large number of articles [13–15]. Ligand binding tendency to biomolecules is critical for biological activity studies. Studies on the interaction of metal complexes with biomolecules to design effective chemotherapeutic agents and better anticancer drugs are essential. During the past decade, a large number of Schiff-base complexes have been synthesized and the interaction of these complexes with serum albumins studied because of their relevance in the development of new therapeutic agents [16–19].

Serum albumins are the most abundant proteins in the plasma. The most important property of this group of proteins is their ability to bind reversibly a large variety of compounds as a depot and a transport protein [20–22]. Also reagents that react with protein chains are very helpful in chemistry and biology [22, 23]. Albumins from blood plasma can bind with a variety of compounds such as pyridoxal phosphate, cysteine, glutathione [24], Schiff-base ligands [25, 26], various metal ions, for example Cu(II), Ni(II) [27], Mn(II), Co(II) [28–30], Hg(II), Zn(II) [27], metal complexes [31], and metallothionein [32]. Bovine serum albumin (BSA) has been one of the most extensively studied group of proteins, especially of its structural homology with human serum albumin [33].

We have studied the interaction of some porphyrazine complexes with biomolecules [34–37]. One disadvantage in bioinorganic studies has been the fact that the synthetic compounds are usually insoluble in water, the normal biological medium, and there is a lack of information about the preparation of water-soluble Schiff-base complexes. Most ligands that are specifically designed for water solubility contain hydrophilic groups such as carboxylate or sulfonate moieties to increase the solubility of such complexes in water [38].

With increasing interest in minimization/elimination of waste and adoption of sustainable processes through green chemistry, and increasing demand for environmentally friendly methods [39], in this work we present a totally green approach toward the synthesis of some new water-soluble quadridentate Schiff-base complexes produced by condensation of the useful starting material salicylaldehyde-5-sulphonate (*sals*) with 2,3-diaminopyridine in the presence of Zn^{2+}, Cu^{2+}, and Ni^{2+}. The mechanism of binding of $Na_2[M(5\text{-}SO_3\text{-}2,3\text{-salpyr})(H_2O)_n]\cdot 2H_2O$ with BSA is investigated by fluorescence spectroscopy. This technique is extensively used for the investigation of ligand binding interaction to proteins. The spectral changes observed on the binding of fluorophores with proteins are an important tool for investigations of the binding sites, conformational changes, and characterization of substrate to ligand binding [40]. Here, the quenching of the intrinsic tryptophan fluorescence of BSA is used as a tool to study the interaction of mentioned complexes with this transport protein under physiological conditions. The values of the Stern–Volmer constants, quenching rate constants, binding constants, binding sites, and average aggregation number of BSA were determined by this method.

In particular, we determined the thermodynamic parameters for the binding of the mentioned complexes to BSA from the van't Hoff equation. Comparison of thermodynamic data leads us to understand the binding mechanism, including hydrophobic interaction. In addition, the conformational change of BSA is discussed on the basis of synchronous fluorescence spectra.

Finally, the mentioned complexes were also screened for their anticancer activities for which the K562 leukemia cell line was the target.

2. Experimental

2.1. *Materials and instruments*

All chemicals were used as obtained commercially without purification.

The NMR spectra were recorded on a Bruker Avance DPX 250 MHz spectrometer. UV-Vis measurements were carried out on Perkin-Elmer (LAMBDA 2) UV-Vis spectrophotometers. Infrared (IR) spectra were recorded on a Shimadzu FTIR 8300 infrared spectrophotometer. Elemental analyses were carried out on a Thermo Fininngan-Flash1200. The metal ions were determined using a Vista-PRO CCD simultaneous ICP-OES instrument. The magnetic measurements were carried out in a vibrating sample magnetometer (BHV-55, Riken, Japan) at room temperature.

All experiments were carried out in triply distilled water at pH = 7.0, 1 mmol L^{-1} phosphate buffer and 5 mmol L^{-1} NaCl. Fluorescence and synchronous fluorescence spectra were recorded on a Cary Eclipse Varian spectrofluorimeter equipped with a thermostated bath at 298, 310, and 318 K.

2.2. *Synthesis and characterization of complexes*

Sodium salicylaldehyde-5-sulfonate monohydrate (*sals*) was synthesized according to the literature procedure [41]; the sulfonation was carried out at 100°C.

2.2.1. Disodium[*N*,*N*′-bis(5-sulphosalicyliden)-2,3-diaminopyridine]zinc(II)dihydrate(Na_2[Zn(5-SO_3-2,3-salpyr)] · $2H_2O$). To a solution of *sals* (0.48 g, 0.002 mol) in water (5 cm^3) was added 2,3-diaminopyridine (0.11 g, 0.001 mol), followed by $Zn(OAc)_2 \cdot 2H_2O$ (0.22 g, 0.001 mol). 1 mol L^{-1} sodium hydroxide was then added to pH 8. The mixture was stirred for 1 h, then ethanol (5 cm^3) was added. The yellow solid was filtered off and washed successively with ethanol. It was recrystallized from ethanol and air-dried.

Yield: 75%; m.p. (>250°C); F.W: 622; Diamagnetic; ^{1}H NMR (250 MHz, D_2O, δ (ppm)): 8.90(s, 1H, H^a), 8.65(s, 1H, H^b), 8.07(d, 1H, $J = 4.5$ Hz, H^c), 7.94–6.61(m, 8H, Ar–H); IR(KBr, cm^{-1}): 3400 $\nu_{(O-H)}$, 2939 $\nu_{(C-H)}$, 1612 $\nu_{(C=N)}$, 1203 $\nu_{(C-O)}$, 1465 $\nu_{(C=C)}$, 1041, 1110, 1173 $\nu_(SO_3^-)$, 458 $\nu_{(M-O)}$; 551 $\nu_{(M-N)}$; Anal. Calcd for $C_{19}H_{15}N_3S_2O_{10}ZnNa_2$ (%): C, 36.76; H, 2.44; N, 6.77; Na, 7.41; Zn, 10.53. Found: C, 36.47; H, 2.36; N, 6.50; Na, 7.32; Zn, 10.58. UV-Vis (H_2O) λ (nm): 430, 390, 310, 250.

2.2.2. Disodium[*N*,*N*′-bis(5-sulphosalicyliden)-2,3-diaminopyridine]nickel(II)dihydrate (Na_2[Ni(5-SO_3-2,3-salpyr)]·$2H_2O$). To a solution of *sals* (0.48 g, 0.002 mol) in water (10 cm^3) was added 2,3-diaminopyridine (0.11 g, 0.001 mol), followed by $Ni(OAc)_2 \cdot 4H_2O$ (0.25 g, 0.001 mol). 1 mol L^{-1} sodium hydroxide was then added to pH 8. The mixture was stirred for 1 h, then ethanol (5 cm^3) added and allowed to stand for 24 h. The orange solid was filtered off and washed successively with ethanol. It was recrystallized and air-dried.

Yield: 80%; m.p. (>250°C); F.W: 614.14; Diamagnetic; ^{1}H NMR (250 MHz, D_2O, δ ppm): 7.85(s, 1H, H^a), 7.65(s, 1H, H^b), 5.62–7.08(m, 9H, Ar–H); IR(KBr, cm^{-1}): 3417 $\nu_{(O-H)}$, 2950 $\nu_{(C-H)}$, 1612 $\nu_{(C=N)}$, 1220 $\nu_{(C-O)}$, 1442 $\nu_{(C=C)}$, 1033, 1110, 1188 $\nu_(SO_3^-)$, 455 $\nu_{(M-O)}$; 563 $\nu_{(M-N)}$; Anal. Calcd for $C_{19}H_{15}N_3S_2O_{10}NiNa_2$ (%): C, 36.10; H, 2.71;

N, 6.65; Na, 7.49; Ni, 9.56. Found: C, 36.98; H, 2.51; N, 6.61; Na, 7.38; Ni, 10.02. UV-Vis (H_2O) λ (nm): 690, 620, 438, 366, 260.

2.2.3. Disodium[diaqua(*N*,*N*′-bis(5-sulphosalicyliden)-2,3-diaminopyridine)]copper(II) dihydrate(Na_2[Cu(5-SO_3-2,3-salpyr)(H_2O)]·2H_2O). To a solution of *sals* (0.48 g, 0.002 mol) in water (10 cm^3) was added 2,3-diaminopyridine (0.11 g, 0.001 mol), followed by $Cu(OAc)_2 \cdot H_2O$ (0.2 g, 0.001 mol). 1 mol L^{-1} sodium hydroxide was then added to pH 8. The mixture was stirred for 1 h, then ethanol (5 cm^3) added and allowed to stand for 48 h. The product was obtained as a brown precipitate, washed successively with ethanol, recrystallized and air-dried.

Yield: 63%; m.p. (>250°C); F.W: 655.01; Paramagnetic (μ: 1.64 B.M); IR(KBr, cm^{-1}): 3420 $\nu_{(O-H)}$, 2990 $\nu_{(C-H)}$, 1606 $\nu_{(C=N)}$, 1220 $\nu_{(C-O)}$, 1450 $\nu_{(C=C)}$, 1034, 1117, 1187 $\nu_{(SO_3^-)}$, 435 $\nu_{(M-O)}$; 555 $\nu_{(M-N)}$; Anal. Calcd for $C_{19}H_{19}N_3S_2O_{12}CuNa_2$ (%): C, 34.84; H, 2.92; N, 6.42; Na, 7.02; Cu, 9.70. Found: C, 35; H, 2.61; N, 6.72; Na, 6.84; Cu, 9.75. UV-Vis (H_2O) λ (nm): 640, 390, 310, 260.

2.3. *Methods*

2.3.1. Fluorescence quenching measurements. The fluorescence spectra were recorded on a Cary Eclipse Varian spectrofluorimeter using 10 nm excitation and 2.5 nm emission slit widths. The samples were placed in quartz cuvettes of 1 cm optical path. In these experiments, 3 mL of BSA solution (10^{-5} mol L^{-1}) were poured into the cell. Emission spectra were recorded after each addition (5 μL) of complex solutions (1.5×10^{-3} mol L^{-1}) in the same buffer at 298, 303, and 310 K. The samples were excited at 280 and 290 nm. The observed fluorescence intensities were also corrected for dilution.

The reaction time has been studied and the results showed that 10s was enough for the stabilization. So the change in fluorescence emission intensity was measured within 10s of adding a complex to BSA.

2.3.2. Synchronous fluorescence spectra measurements. The synchronous fluorescence spectra were obtained by scanning simultaneously the excitation and emission monochromator with a Cary Eclipse Varian spectrofluorimeter. The synchronous fluorescence spectra only show the tyrosine residues and the tryptophan residue of BSA when the wavelength interval (Δλ) is 15 nm and 60 nm, respectively [42].

2.3.3. Cell line. Human immortalized myelogenous leukemia cell line K562 was obtained from the cell bank of Pasteur Institute of Iran. These cells were maintained in RPMI 1640 medium, supplemented with 10% heat-inactivated fetal calf serum, 1% penicillin–streptomycin (100 mg mL^{-1} streptomycin and 100 U mL^{-1} penicillin) in a humidified incubator (37°C and 5% CO_2).

2.3.4. The cell proliferation assay. The growth inhibitory effects of the complexes toward the K562 cancer cell line was measured by 3-(4,5-dimethylthiazol-2-Yl)-2,5-diphenyltetrazolium bromide (MTT) assay [43]. A certain number of cancer cells

(2.5×10^4 cells mL^{-1}) was seeded in the wells of a 96-well plate with varying concentrations of the complexes (0–100 μmol L^{-1}) and incubated for 24 h. After 4 h to the end of incubation, 25 µL of MTT solution (5 mg mL^{-1} in PBS) was added to each well containing fresh and cultured medium. At the end, the insoluble formazan produced was dissolved in a solution containing 10% SDS and 50% DMF (left for 2 h at 37°C in the dark) and the optical density (OD) was read against reagent blank with a multi-well scanning spectrophotometer (ELISA reader, Bio-Tek's ELx808, USA) at a wavelength of 570 nm. The absorbance is a function of concentration of the converted dye. The OD value of the studied groups was divided by the OD value of the untreated control and presented as percentage of control (as 100%) [44].

2.3.5. Statistical analysis. The cell culture experiments were repeated three times for each sample, and the statistical differences were determined by analysis of variance (ANOVA) followed by Turkey–Kramer multiple comparison tests on the instant package. Differences were regarded as significant at $P < 0.05$.

3. Results and discussion

3.1. *Synthesis and characterization of complexes*

The Schiff-base complexes were synthesized by the template method and their structures characterized by elemental analyses, ^{1}H NMR, TGA, IR, UV-Vis spectra, and magnetic susceptibility measurement. The elemental analyses show that the ratio of metal/L in all complexes is 1 : 1; the likely structures of the complexes are shown in figure 1. All complexes are air stable for extended periods and soluble in water, slightly soluble in methanol, ethanol, and DMSO and insoluble in non-polar solvents.

3.2. *IR spectra*

IR spectral data for the complexes are given in section 2. The vibration band for the complexes around 3400 cm^{-1} is attributed to the presence of lattice and coordinated water [45]. Medium-weak bands at 2990 and 3050 cm^{-1} are observed for the aromatic (C–H) stretching bands. The Schiff-base structure of the *N*,*N*′-bis(5-sulphosalicyliden)-

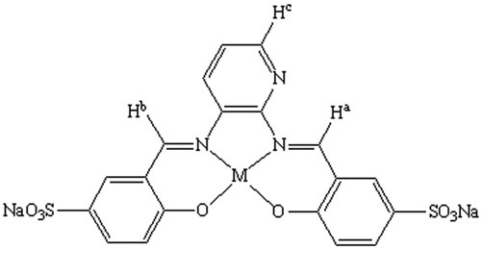

Figure 1. Structure of the water-soluble Schiff-base complexes $Na_2M(5\text{-}SO_3\text{-}2,3\text{-salpyr})]$, M = Zn, Cu, and Ni.

2,3-diaminopyridine moiety of the obtained compounds is indicated by the presence of strong imine (C=N) bands at 1600 cm^{-1} [46]. The phenolic (C–O) stretching bands, because of the participation of oxygen in the C–O–M bond, are observed at 1200–1220 cm^{-1}.

The ring skeletal vibrations (C=C) were consistent in the region of 1440–1465 in all complexes [47]. A medium-strong band present at 1525–1560 cm^{-1} due to vibration of (Ph–)C–C(=N) [48] typifies complexes derived from salicylaldehyde [49]. Three peaks around 1200, 1100 and 1040 cm^{-1} are related to the SO_3 group [47].

In the lower frequency region medium-weak bands observed at 551–563 and 435–458 cm^{-1} have been assigned to (M–N) and (M–O) vibrations, respectively [50, 51].

3.3. *Electronic spectra, magnetic susceptibility measurement, and ^1H NMR spectroscopy*

Electronic spectral data for the complexes in water are given in section 2. These complexes show intense absorptions at 220–370 nm, attributed to the $\pi \rightarrow \pi^*$ transition in aromatic rings or azomethine groups and $n \rightarrow \pi^*$ transition in the pyridine ring. In the electronic spectra of all complexes the LMCT band at 390–450 nm can be observed. Absorptions observed between 600 and 800 nm can be attributed to d–d transitions of the metal ions. These smaller values of the wavelengths have particular importance because they are highly dependent on the geometry of the molecule.

The spectrum of the Ni(II) complex showed broad and weak absorption bands at 620 and 690 nm ascribed to $^1A_{1g} \rightarrow {}^1B_{1g}$ and $^1A_{1g} \rightarrow {}^1A_{2g}$ transitions, respectively, supporting square-planar geometry. The Cu(II) complex shows a broad and low energy band at 640 nm which may be assigned to the $^2B_{1g} \rightarrow {}^2A_{1g}$ transition in square-planar geometry around copper [52]. Zn(II) complexes do not exhibit d–d electronic transitions.

The magnetic susceptibility results of the transition metal complexes also give an indication of the geometry of the ligands around the metal. The zinc and nickel complexes were diamagnetic and the copper complex was paramagnetic (μ: 1.64 B.M), which was within the range normally observed for square-planar Cu(II) complexes corresponding to d^9 configuration in a magnetically dilute environment. ^1H NMR spectral data of the zinc and nickel complexes are given in section 2. The pyridyl and aromatic protons were observed in the range ~5.6–7.9 ppm and two sets of resonances were observed for azomethine protons, which show they are in a different chemical environment. The signals for these protons were observed in the ~7.6–8.9 ppm range. ^1H NMR spectral data of the copper complex gave no signal due to their paramagnetism.

3.4. *Thermal analysis*

The thermal studies were carried out using thermogravimetric analysis (TGA) and derivative thermogravimetric techniques. The decomposition mass losses were in accord with the molecular weight of each complex proposed from the elemental analysis. The decomposition patterns were further confirmed from mass spectral peaks. The hydrated water molecules are associated with complex formation and found in the outer coordination sphere. The dehydration occurs from 25–220°C. Coordinated water

Table 1. Thermogravimetric data of metal complexes.

Compound	Temperature (°C)	DTA (peak)		TGA (Wt. loss %)		Assignment
		Endo	Exo	Calcd	Found	
$Na_2[Zn(L)]\cdot 2H_2O$	80	Endo	–	5.7	5.6	Loss of hydrated water ($2H_2O$)
	100	–	Exo	7.4	7.2	Loss of sodium ions ($2Na^+$)
	450	–	Exo	73.4	74.0	Decomposition of ligand with formation of ZnO
$Na_2[Ni(L)]\cdot 2H_2O$	75	Endo	–	5.8	5.7	Loss of hydrated water ($2H_2O$)
	100	–	Exo	7.5	7.8	Loss of sodium ions ($2Na^+$)
	450	–	Exo	74.5	73.0	Decomposition of ligand with formation of NiO
$Na_2[Cu(L)(H_2O)_2]\cdot 2H_2O$	75	Endo	–	5.5	5.6	Loss of hydrated water ($2H_2O$)
	110	Endo	–	5.5	5.46	Loss of coordinated water ($2H_2O$)
	150	–	Exo	7.0	6.9	Loss of sodium ions ($2Na^+$)
	400	–	Exo	69.8	68.0	Decomposition of ligand with formation of CuO

molecules are eliminated at higher temperatures of 100–316°C. The mass loss between 150 and 400°C was assigned to loss of sodium ions. The organic part of the complexes decomposes in one or more steps with the formation of one or two intermediates. These intermediates may finally decompose to stable metal oxides [53]. The results of TGA and DTA data for all complexes are summarized in table 1. The outcome confirmed that the products are stable to 400°C, where the organic residues of the complexes start to decompose.

3.5. *Fluorescence spectroscopy*

Fluorescence quenching refers to any process, which decreases the fluorescence intensity of a sample. A variety of molecular interactions can result in quenching, including excited-state reactions, molecular rearrangements, energy transfer, ground-state complex-formation, and collisional quenching.

To interpret the data from fluorescence quenching studies, it is important to understand the interaction between the fluorophore (BSA) and the quencher (Na_2[M(5-SO_3-2,3-salpyr)]).

Usually, quenching occurs by two mechanisms, collisional process (dynamic quenching) or formation of a complex between the quencher and the fluorophore (static quenching). These two quenching mechanisms are distinguishable by their differing dependence on viscosity and temperature. The dynamic quenching mechanism depends upon diffusion. Since higher temperatures result in larger diffusion coefficients, the quenching rate constants are expected to increase with increasing temperature. But, increased temperature is likely to result in lower values of the static quenching constants.

The stepwise addition of Na_2[Zn(5-SO_3-2,3-salpyr)] to BSA in 0.1 mol L^{-1} phosphate buffer (pH = 7.0) resulted in progressive quenching of the intensity at all wavelengths, as shown in figure 2. Similar situations were observed for the other complexes.

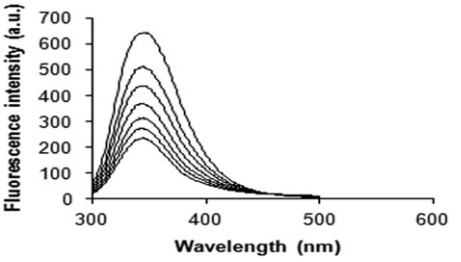

Figure 2. Effect of water-soluble Schiff-base complex, $Na_2[Zn(5\text{-}SO_3\text{-}2,3\text{-salpyr})]$, on the fluorescence spectra of BSA ($T = 298$ K). [BSA] $= 1.0 \times 10^{-5}$ mol dm^{-3}, [$Na_2[Zn(5\text{-}SO_3\text{-}2,3\text{-salpyr})] = 2.5 \times 10^{-6}$–$2.0 \times 10^{-5}$ mol dm^{-3}. The emission intensity is decreased due to increasing $Na_2[Zn(5\text{-}SO_3\text{-}2,3\text{-salpyr})]$ concentration.

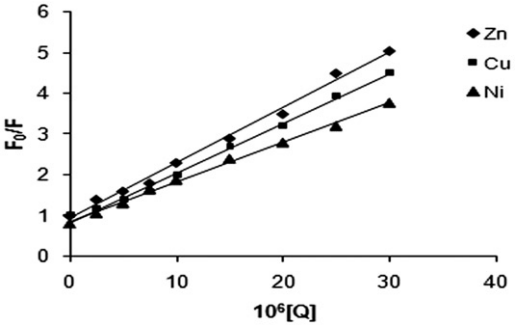

Figure 3. The Stern–Volmer plots of BSA (1.0×10^{-5} mol dm^{-3}) binding to $Na_2[M(5\text{-}SO_3\text{-}2,3\text{-salpyr})]$, $\lambda_{Ex} = 290$ nm, $\lambda_{Em} = 344$ nm.

The fluorescence quenching data were plotted as relative fluorescence intensity (RFI $= F/F_0$) *versus* $Na_2[M(5\text{-}SO_3\text{-}2,3\text{-salpyr})]$ concentration. Fluorescence quenching is described by the Stern–Volmer equation [54]:

$$\frac{F_0}{F} = 1 + K_{SV}[Q] = 1 + k_q\tau_0[Q], \tag{1}$$

where F and F_0 are the luminescence intensities in the presence and absence of quencher, respectively, $[Q]$ is the quencher concentration and K_{SV}, the Stern–Volmer constant, is the product between the quenching rate constant (k_q) and luminescence lifetime of the fluorophore in the absence of quencher (τ_0) (for BSA, the lifetime of the fluorophore is approximately 5 ns [54]). Linear Stern–Volmer plots shown in figure 3 indicate that equation (1) is applicable for the present systems.

The average BSA aggregation number, $\langle J \rangle$, potentially induced by complexes can be determined by using equation (2):

$$1 - \frac{F}{F_0} = \langle J \rangle \frac{[Q]}{[\mathrm{BSA}]_0}. \tag{2}$$

The slopes ($\langle J \rangle$) of the lines in figure 4 (table 2) are less than one for all complexes, showing that the complex binding does not induce aggregation in BSA molecules and prove the 1 : 1 stoichiometry for the $Na_2[M(5\text{-}SO_3\text{-}2,3\text{-salpyr})]$: BSA systems.

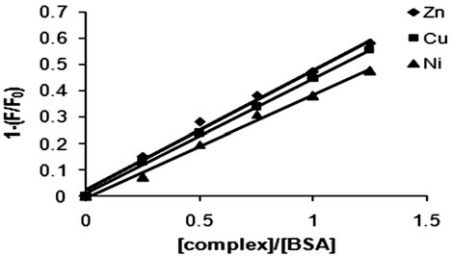

Figure 4. Determination of the average aggregation number of BSA ($\langle J \rangle$) in the presence of Na_2[M(5-SO_3-2,3-salpyr)]. $\lambda_{Ex} = 290$ nm, $\lambda_{Em} = 344$ nm, and the spectral band widths are 5 nm for both excitation and emission slits.

Table 2. The values of Stern–Volmer quenching constants (K_{sv}), quenching rate constant (k_q), modified Stern–Volmer constant (K_a), and average aggregation number of BSA molecules ($\langle J \rangle$) for the interaction of metal complexes with BSA at different temperatures.

Compound	T (K)	K_{sv} ($\times 10^5$ dm^3 mol^{-1})	k_q ($\times 10^{13}$ dm^3 mol^{-1}S^{-1})	K_a ($\times 10^5$ dm^3 mol^{-1})	
$Na_2[Zn(L)] \cdot 2H_2O$	298	1.2155	2.4312	1.1192	0.45
	303	1.0136	2.0272	0.9769	
	310	0.8667	1.7335	0.8245	
$Na_2[Cu(L)(H_2O)_2] \cdot 2H_2O$	298	1.1960	2.3921	1.0340	0.43
	303	0.9604	1.9209	0.8204	
	310	0.9355	1.8711	0.7905	
$Na_2[Ni(L)] \cdot 2H_2O$	298	0.9914	1.9829	0.9840	0.39
	303	0.9638	1.9277	0.9308	
	310	0.9271	1.8542	0.7725	

The values of K_{SV} listed in table 2 represent the relative affinity of Na_2[M(5-SO_3-2,3-salpyr)] for BSA. The obtained k_q values in table 2 are 10^3 higher than the maximum value possible for the diffusion limited quenching of various kinds of quenchers with biopolymers in aqueous solution, i.e., $k_{diff} = 2 \times 10^{10}$ $(\text{mol L}^{-1})^{-1}\,\text{s}^{-1}$ [55], which suggests that the quenching is not initiated by dynamic collision and that there is complex-formation between BSA and Na_2[M(5-SO_3-2,3-salpyr)]. The results show that the Stern–Volmer quenching constant K_{SV} at different temperatures (298, 303, and 310 K) is inversely correlated with temperature. These findings confirm that quenching mechanism of Na_2[M(5-SO_3-2,3-salpyr)]-BSA binding is initiated by complex formation with BSA rather than by dynamic collision.

The calculation of K_{SV} from Stern–Volmer plots demonstrates that varying temperature has a moderate effect on the fluorescence quenching by Na_2[M(5-SO_3-2,3-salpyr)]. Therefore, the quenching data were analyzed according to the modified Stern–Volmer equation [56]:

$$\frac{F_0}{\Delta F} = \frac{1}{f_a K_a}\frac{1}{[Q]} + \frac{1}{f_a}. \tag{3}$$

In this case, ΔF is the difference in fluorescence in the absence and presence of the quencher at the concentration $[Q]$, f_a is the mol fraction of the initial fluorescence,

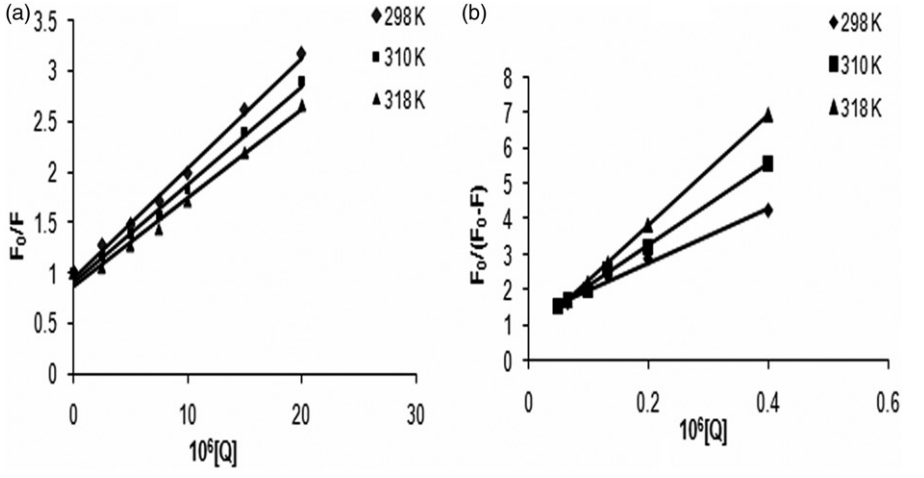

Figure 5. Stern–Volmer plots (a) and modified Stern–Volmer plots (b) for the quenching of BSA by Na_2[Cu(5-SO_3-2,3-salpyr)] at different temperatures.

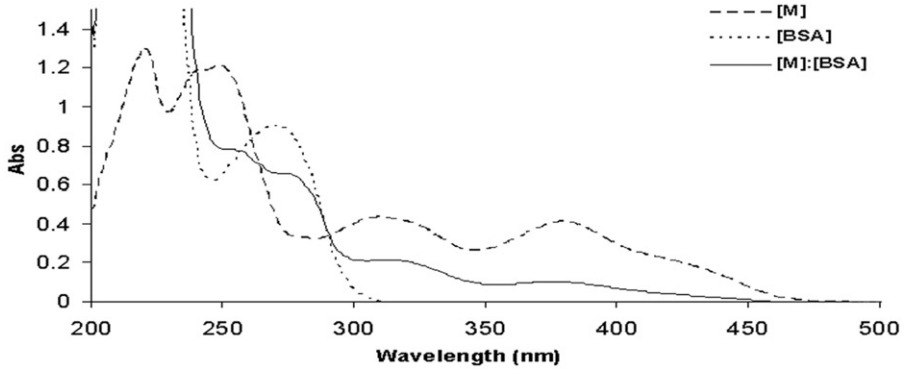

Figure 6. UV-Vis spectra of Na_2[Zn(5-SO_3-2,3-salpyr)] (2.0×10^{-5} mol dm^{-3}), [BSA] (2.0×10^{-5} mol dm^{-3}) and 1 : 1 Na_2[Zn(5-SO_3-2,3-salpyr)]-BSA adduct in equilibrium with each other.

which is available to the quencher, and K_a is the effective quenching constant for the accessible fluorophores. The dependence of $F_0/\Delta F$ on the reciprocal value of the quencher concentration $[Q]^{-1}$ is linear with the slope of $(f_a K_a)^{-1}$. The effective quenching constant (K_a) is a quotient of an ordinate f_a^{-1} and the slope $(f_a K_a)^{-1}$. Stern–Volmer plots and modified Stern–Volmer plots for the quenching of BSA by Na_2[Zn(5-SO_3-2,3-salpyr)] at different temperatures in figure 5 are compared, and also the modified quenching constants K_a at different temperatures are shown in table 2. The decreasing trend in K_a with increasing temperature was in accord with K_{SV}'s dependence on the temperature as mentioned above, confirming our suggestion about the quenching mechanism [54]. UV-Vis absorption spectra of BSA, Na_2[Zn(5-SO_3-2,3-salpyr)], and the Na_2[Zn(5-SO_3-2,3-salpyr)]–BSA adduct (figure 6) are in

Table 3. Apparent binding constant, binding site, and thermodynamic parameters for the interaction of metal complexes with BSA at different temperatures.

Compound	T (K)	K_b ($\times 10^6$ dm^3 mol^{-1})	Binding sites (n)	ΔH (kJ mol^{-1})	ΔS (J mol^{-1} K^{-1})	ΔG (kJ mol^{-1})
[Zn(L)]	298	0.50118	1.13	220.6 ± 6.1	849.22 ± 8.4	−32.44
	303	1.99526	1.15			−36.68
	310	15.61349	1.19			−42.63
[Cu(L)]	298	0.212275	1.06	292.4 ± 5.6	1080.9 ± 9.3	−29.44
	303	1.135534	1.12			−34.84
	310	6.309573	1.06			−42.40
[Ni(L)]	298	0.123026	1.00	51.93 ± 1.58	271.78 ± 5.2	−29.05
	303	0.177827	1.06			−30.42
	310	0.277523	1.09			−32.32

accord with the static quenching mechanism. Similar results have been seen for systems containing Cu and Ni.

3.6. *Determination of the binding constant and the binding site*

In the static quenching interaction [57], if there are multiple equivalent (but independent) binding sites for a quencher (Q) in a biomolecule (B) to form a complex Q_nB (equation (4)), the binding constant K_b is given by equation (5):

$$nQ + B \rightarrow Q_nB, \tag{4}$$

$$k_b = \frac{[Q_nB]}{[Q]^n[B]}. \tag{5}$$

In the present case, $[B_0]$ is the total amount of biomolecule (with and without bound Q), this means $[B_0] = [Q_nB] + [B]$, and $[B]$ is the concentration of the unbound biomolecule. Since $[B]/[B_0] = F/F_0$, the relationship between the fluorescence intensity and the unbound biomolecule is expressed as

$$\log\left(\frac{F_0 - F}{F}\right) = \log k_b + n \log[Q], \tag{6}$$

where F_0 and F are the fluorescence intensities in the absence and presence of Na_2[M(5-SO_3-2,3-salpyr)], K_b is the apparent binding constant of Na_2[M(5-SO_3-2,3-salpyr)] with BSA, and n is the number of binding sites per BSA. Table 3 gives the results of K_b and n at different temperatures analyzed in this method for BSA.

3.7. *Comparing reactions between phenylbutazone and Na_2[M(5-SO_3-2,3-salpyr)] for binding to BSA*

BSA has two main sites for binding to drugs: (i) site I of BSA where the tryptophan residue binds to drugs and (ii) site II where tyrosine is located. While 290 nm light

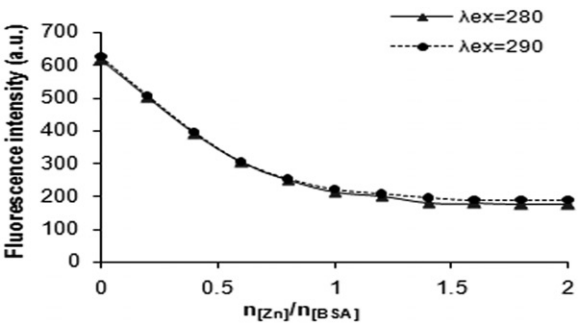

Figure 7. Fluorescence changes of BSA (1.0×10^{-5} mol dm^{-3}) by [Na_2[Zn(5-SO_3-2,3-salpyr)] (2.5×10^{-6}–2.0×10^{-5} mol dm^{-3}), $\lambda_{Ex} = 280$ nm (continuous line), $\lambda_{Ex} = 290$ nm (dashed line), and $\lambda_{Em} = 344$ nm for both.

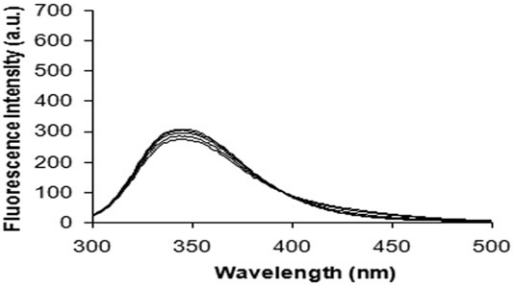

Figure 8. Quenching effect of BSA (1.0×10^{-5} mol dm^{-3}) binding to [Na_2[Zn(5-SO_3-2,3-salpyr)] (2.5×10^{-6}–2.0×10^{-5} mol dm^{-3}) in the presence of phenyl butazone (1.0×10^{-4} mol dm^{-3} in 50 : 50 V/V water/acetone).

excites tryptophan residues, 280 nm light excites both tryptophan and tyrosine residues [54]. Comparing the quenching effects, when BSA was excited at 290 and 280 nm (figure 7), confirms that only the tryptophan of BSA binds with Na_2[M(5-SO_3-2,3-salpyr)]. Thus, the major binding site for Na_2[M(5-SO_3-2,3-salpyr)] is site I of this protein, which is located in subdomain IIA where tryptophan 212 is and there is a large hydrophobic cavity [58–60]. In order to show Na_2[M(5-SO_3-2,3-salpyr)] binding to the tryptophan residue, we used phenylbutazone as a well-known site marker for site I [54]. A mixture of equal amounts of BSA and phenylbutazone (5.00×10^{-5} mol L^{-1} in 50 : 50 V/V% water/acetone) was titrated by Na_2[M(5-SO_3-2,3-salpyr)] solution. The results show that the quenching of BSA in the presence of phenylbutazone is very small (figure 8). Based on these results, we deduce that a competition exists for the binding of phenylbutazone and Na_2[M(5-SO_3-2,3-salpyr)] to site I. Therefore, Na_2[M(5-SO_3-2,3-salpyr)] binding to site I is inhibited by simultaneous binding of the site I ligand. These findings confirm our suggestion about Na_2[M(5-SO_3-2,3-salpyr)] binding to site I of BSA.

Since a large hydrophobic cavity is present in IIA subdomain, Na_2[M(5-SO_3-2,3-salpyr)]–BSA interaction is predominantly hydrophobic. These results are also confirmed by thermodynamic results.

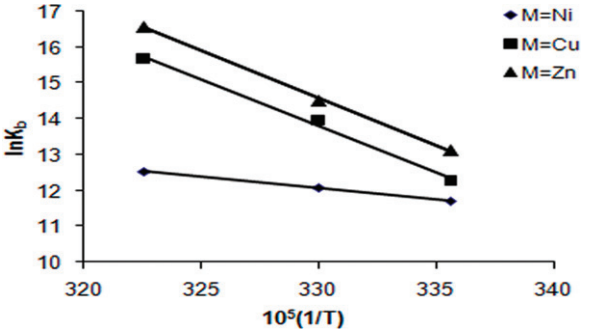

Figure 9. The van't Hoff plots of BSA binding to Na_2[M(5-SO_3-2,3-salpyr)], M = Zn, Cu, and Ni.

3.8. *Determination of the thermodynamic parameters and the nature of the binding site between Na_2[M(5-SO_3-2,3-salpyr)] and BSA*

The forces enabling the binding of one compound as a drug with proteins are composed of various weak non-covalent interactions including hydrophobic, electrostatic, hydrogen-bonding, and van der Waals interactions. To obtain further insights into the weak interactions associated with the complexation of Na_2[M(5-SO_3-2,3-salpyr)] with BSA, we endeavored to determine the thermodynamic parameters by using the van't Hoff equation [61]:

$$\ln K = -\frac{\Delta H}{RT} + \frac{\Delta S}{R}, \tag{7}$$

where K is the binding constant at the corresponding temperature and R is the gas constant. The van't Hoff plots for this interaction (figure 9) indicate that there is a good linear relationship between $\ln K$ and $1/T$. The enthalpy change (ΔH) is calculated from the slope of the van't Hoff relationship. The free energy change (ΔG) is estimated from the following relationship:

$$\Delta G = \Delta H - T\Delta S. \tag{8}$$

Ross and Subramanian [62] have used the sign and magnitude of the thermodynamic parameters to decide the nature of the interaction in a variety of host–guest systems. Such host–guest systems associated with $\Delta H > 0$ and $\Delta S > 0$ are driven by hydrophobic interactions, while those with $\Delta H \approx 0$ and $\Delta S > 0$ by electrostatic interactions, and those with $\Delta H < 0$ and $\Delta S < 0$ by hydrogen-bonding or van der Waals interactions. Here, the positive values of ΔH and ΔS indicate that hydrophobic interactions play a major role in the binding reaction [62]. Certainly, unfavorable enthalpy values are cancelled out by the much larger entropy gain ($T\Delta S > \Delta H$), probably derived from the extensive dehydration of Na_2[M(5-SO_3-2,3-salpyr)] and BSA, to provide a very stable complex with large K_a values (table 2). Also the negative values of the free energy (ΔG) prove that the binding process is spontaneous.

3.9. *Energy transfer between Na_2[M(5-SO_3-2,3-salpyr)] and BSA*

The spectral properties of BSA to Na_2[M(5-SO_3-2,3-salpyr)] are ideal for an efficient fluorescence resonance energy transfer wherein BSA acts as donor and Na_2[M(5-SO_3-2,3-salpyr)] as acceptor.

The energy transfer efficiency between $Na_2[M(5\text{-}SO_3\text{-}2,3\text{-salpyr})]$ and BSA was studied according to Förster's energy transfer theory [63]. The Förster theory shows that energy transfer is affected not only by the distance between the acceptor and the donor, but also by the critical distance of energy transfer (R_0), which can be calculated using the following equation:

$$E = \frac{R_0^6}{R_0^6 + r^6} = 1 - \frac{F}{F_0}, \tag{9}$$

where F and F_0 are the fluorescence intensities of the biomolecule in the presence and absence of quencher, r the donor–acceptor distance and R_0 the critical distance where the transfer efficiency is 50%:

$$R_0^6 = 8.8 \times 10^{-25} K^2 N^{-4} \Phi J, \tag{10}$$

where K^2 is the space factor of orientation, N the refractive index of the medium, Φ the fluorescence quantum yield of donor, J the effect of the spectral overlap between the emission spectrum of the donor, and the absorption spectrum of the acceptor, calculated as

$$J = \frac{\int_0^\infty F(\lambda)\epsilon(\lambda)\lambda^4 \mathrm{d}\lambda}{\int_0^\infty F(\lambda)\mathrm{d}\lambda}, \tag{11}$$

where $F(\lambda)$ is the corrected fluorescence intensity of the donor in the wavelength range of λ to $(1+\Delta\lambda)$ and $\epsilon(\lambda)$ the molar extinction coefficient of the acceptor at λ. Figure 10 shows the overlap of the UV-Vis absorption spectrum of $Na_2[M(5\text{-}SO_3\text{-}2,3\text{-salpyr})]$ with the fluorescence emission spectrum of BSA. In this case, $K^2 = 2/3$, $N = 1.36$, and $\Phi = 0.15$ for BSA [64]. According to equations (9)–(11), the corresponding results are shown in table 4. Since the average distance $r < 7$ nm [65] and $0.5R_0 < r < 1.5R_0$ [66], the energy transfer from BSA to $Na_2[M(5\text{-}SO_3\text{-}2,3\text{-salpyr})]$ occurred with high probability. These results indicate again the static quenching interaction between $Na_2[M(5\text{-}SO_3\text{-}2,3\text{-salpyr})]$ and BSA.

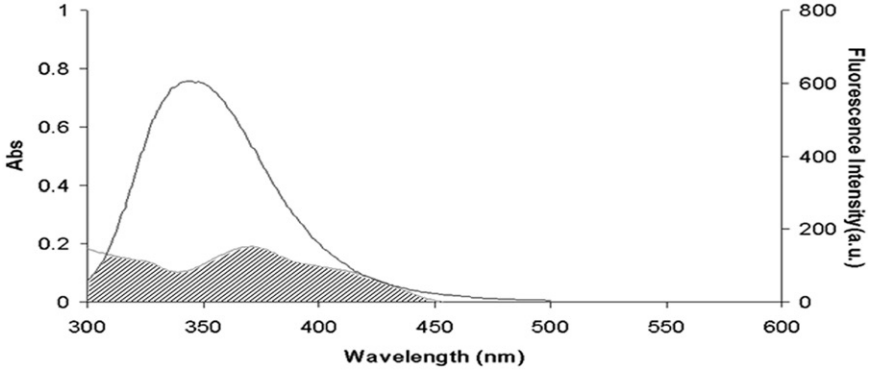

Figure 10. Spectral overlap of $Na_2[Zn(5\text{-}SO_3\text{-}2,3\text{-salpyr})]$ absorption (a) with BSA fluorescence (b); $C(BSA) = C$ $(Na_2[Zn(5\text{-}SO_3\text{-}2,3\text{-salpyr})]) = 1.0 \times 10^{-5}$ mol dm^{-3} ($T = 298$ K).

3.10. *Effect of $Na_2[M(5\text{-}SO_3\text{-}2,3\text{-salpyr})]$ on the protein conformation*

Fluorescence of BSA comes from the tyrosine, tryptophan, and phenylalanine residues, sensitive to the micro-environment of these chromophores allowing non-intrusive measurements of protein under physiological conditions.

The changes in maximum emission wavelength of the tryptophan residues reflect the conformation changes of BSA. From figure 2, the emission of BSA does not shift with increasing concentration of $Na_2[Zn(5\text{-}SO_3\text{-}2,3\text{-salpyr})]$. When considering the effect of $Na_2[Zn(5\text{-}SO_3\text{-}2,3\text{-salpyr})]$ on the fluorescence spectra of BSA, the maximal emission wavelength of BSA does not shift, suggesting no other change in the immediate environment of the tryptophan residues except the fact that $Na_2[Zn(5\text{-}SO_3\text{-}2,3\text{-salpyr})]$ is situated at close proximity to the tryptophan residue for the quenching effect to occur.

The observation that the protein conformation was not affected obviously with addition of $Na_2[M(5\text{-}SO_3\text{-}2,3\text{-salpyr})]$ was also demonstrated by synchronous fluorescence spectra. In synchronous fluorescence spectroscopy according to Miller [67], distinction of the difference between excitation wavelength and emission wavelength ($\Delta\lambda$) reflects the spectra of disparate chromophores; with large $\Delta\lambda$ values such as 60 nm, the synchronous fluorescence of BSA is characteristic of tryptophan residue and with small $\Delta\lambda$ values such as 15 nm is characteristic of tyrosine. The tyrosine residues and the tryptophan residues of the fluorescence spectra of BSA at various concentrations of $Na_2[Zn(5\text{-}SO_3\text{-}2,3\text{-salpyr})]$ are shown in figure 11(a) and (b), respectively. The quenching of the fluorescence intensity of tryptophan residues is

Table 4. Energy transfer parameters for the interaction of metal complexes with BSA

Compound	R_0 (nm)	r (nm)	J ($cm^3\,L\,mol^{-1}$)	E
[Zn(L)]	2.89	2.86	2.28×10^{-14}	0.51
[Cu(L)]	2.82	2.85	1.94×10^{-14}	0.48
[Ni(L)]]	2.95	2.96	2.56×10^{-14}	0.49

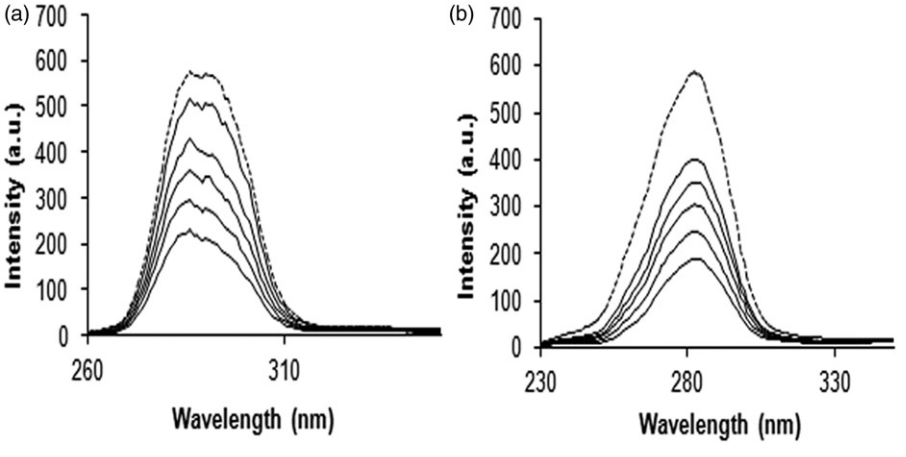

Figure 11. Synchronous fluorescence spectra of BSA ($1.00 \times 10^{-5}\,mol\,L^{-1}$) with $\Delta\lambda = 15$ nm (a) and $\Delta\lambda = 60$ nm (b) in the absence (dotted lines) and presence of $Na_2[Zn(5\text{-}SO_3\text{-}2,3\text{-salpyr})]$ (2.0×10^{-6}–1.0×10^{-5}) (solid lines).

stronger than that of the tyrosine residue, suggesting that tryptophan residues contribute to the quenching of the intrinsic fluorescence.

No significant shift change on the wavelength was observed, indicating that the interaction of Na_2[Zn(5-SO_3-2,3-salpyr)] with BSA does not affect the conformation of the tryptophan and tyrosine micro-regions. Similar spectral features were observed for the interaction of Na_2[Cu(5-SO_3-2,3-salpyr)] and Na_2[Ni(5-SO_3-2,3-salpyr)] with BSA.

3.11. *Evaluation of growth inhibitory activity of the Schiff-base complexes against K562 cancer cell line*

The anticancer properties of Schiff-base complexes have already been proven [6–10]. In this study, the synthetic water-soluble Schiff-base complexes were screened for their anticancer activities for which the K562 leukemia cell line was the target. The cancer cells (2.5×10^4 cells mL^{-1}) were incubated in the presence of increasing concentration of the complexes (0–100 μmol L^{-1}) for 24 h, and the anti-proliferation activity was measured according to the procedure described in sections 2.1 and 2.3. As shown in figure 12, these complexes revealed significant anti-proliferation activity against the cancer cell line in the range 0–100 μmol L^{-1}. Moreover, the growth inhibitory activities of the metal complexes were [Cu] > [Zn] > [Ni].

These results indicate that these complexes can be a potential anticancer agent and further investigation needs to reveal more on their mode of action. Various anticancer drugs induce cell death by induction of oxidative stress and generation of reactive oxygen species in the target cells [68, 69].

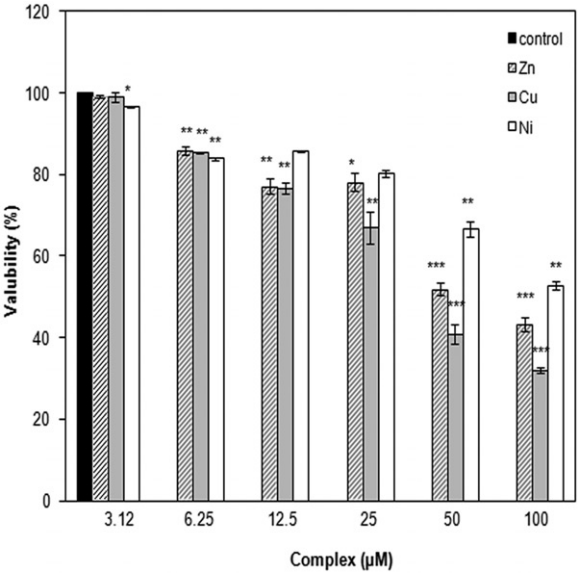

Figure 12. The anti-proliferation activity of the Schiff-base complexes; the vertical bars represent standard deviation of triplicate determinations while the asterisks indicate *$p < 0.05$, **$p < 0.01$, and ***$p < 0.001$, as the anti-proliferation activities of the complexes were compared to the control experiments (absence of any cytotoxic agent).

4. Conclusions

New water-soluble Schiff-base complexes were synthesized *via* the template method. These syntheses were conducted using environmentally friendly methods in water and do not require harsh bases or acids. The formulations were in agreement with the data of elemental analysis, magnetic susceptibility measurement, IR, ^{1}H NMR, TGA, and UV-Vis spectroscopy.

We investigated the interaction of the complexes with BSA by a spectrofluorimetric method. The fluorescence of BSA mostly originates from the tryptophan residues, which can be quenched by the complexes, and the results show that the probable quenching mechanism is a static process. Complex binding does not induce any aggregation in the BSA molecules and proved the 1 : 1 stoichiometry for the Na_2[M(5-SO_3-2,3-salpyr)]: BSA systems. The micro-environment around the tryptophan residues does not show obvious changes during the binding process.

Thermodynamic results indicate that the binding process is endothermic and essentially entropy-driven, suggesting that hydrophobic interactions play a significant role in adduct formation, and the high affinity of BSA for these complexes is clearly evidenced by ΔG values which clarifies the role of albumin as endogenous carrier for these complexes in the body, which could be a useful guide for further drug design.

Finally, the complexes were also screened for their anticancer activities for which the K562 leukemia cell line was the target. The growth inhibitory activities of the metal complexes were [Cu] > [Zn] > [Ni].

References

[1] C.M. da Silva, D.L. da Silva, L.V. Modolo, R.B. Alves, M.A. de Resende, C.V.B. Martins, A. Fatima. *J. Adv. Res.*, **2**, 1 (2011).
[2] N. Raman, A. Kulandaisamy, C. Thangaraja. *Transition Met. Chem.*, **29**, 129 (2004).
[3] S.N. Pandeya, D. Sriram, G. Nath, E. DeClercq. *Eur. J. Pharm. Sci.*, **9**, 25 (1999).
[4] P. Panneerselvam, R.B. Nair, G. Vijayalakshmi, E.H. Subramanian, S.K. Sridhar. *Eur. J. Med. Chem.*, **40**, 225 (2005).
[5] S.K. Sridhar, M. Saravanan, A. Ramesh. *Eur. J. Med. Chem.*, **36**, 615 (2001).
[6] S.H. Etaiw, D.M. Abd El-Aziz, E.H. Abd El-Zaher, E.A. Ali. *Spectrochim. Acta, Part A*, **79**, 1331 (2011).
[7] X. Zhong, J. Yi, J. Sun, H.L. Wei, W.S. Liu, KB. Yu. *Eur. J. Med. Chem.*, **41**, 1090 (2006).
[8] Z.Y. Yang, R.D. Yang, F.S. Li, K.B. Yu. *Polyhedron*, **19**, 2599 (2000).
[9] R. Mladenova, M. Ignatova, N. Manolova, T. Petrova, I. Rashkov. *Eur. Polym. J.*, **38**, 989 (2002).
[10] O.M. Walsh, M.J. Meegan, R.M. Prendergast, T.A. Nakib. *Eur. J. Med. Chem.*, **31**, 989 (1996).
[11] R. Atkins, G. Brewer, E. Kokot, G.M. Mockler, E. Sinn. *Inorg. Chem.*, **24**, 127 (1985).
[12] J.E. Kovacic. *Spectrochim. Acta*, **23A**, 183 (1967).
[13] A. Sigel. In *Metal Ions in Biological Systems*, H. Sigel (Ed.), Vol. 32, Marcel Dekker, New York (1996).
[14] K.E. Erkkila, D.T. Odom, J.K. Barton. *Chem. Rev.*, **99**, 2777 (1999).
[15] C. Metcalfe, J.A. Thomas. *Chem. Soc. Rev.*, **32**, 215 (2003).
[16] Q. Xiao, S. Huang, Y. Liu, F.-F. Tian, J.-C. Zhu. *J. Fluoresc.*, **19**, 317 (2009).
[17] H.Y. Shrivastava, B.U. Nair. *J. Inorg. Biochem.*, **98**, 991 (2004).
[18] D.M. Boghaei, M. Gharagozlou. *Spectrochim. Acta, Part A*, **66**, 650 (2007).
[19] Y. Xiang, F. Wu. *Spectrochim. Acta, Part A*, **77**, 430 (2010).
[20] W.A. Schroeder. *J. Am. Chem. Soc.*, **80**, 3802 (1958).
[21] W.E. Klopfenstein. *Biochem. Biophys. Acta*, **181**, 323 (1969).
[22] W.G. Unger. *J. Pharm. Pharmacol.*, **24**, 470 (1972).
[23] A. Schepartz, B. Cuenoud. *J. Am. Chem. Soc.*, **112**, 3247 (1990).
[24] J.S. Stamler, D.J. Singel, J. Loscalzo. *Science*, **258**, 1898 (1992).
[25] H.Y. Shrivastava, M. Kanthimathi, B.U. Niar. *Biochem. Biophys. Res. Commun.*, **265**, 311 (1999).

[26] J. Gao, Y. Guoa, J. Wang, Z. Wang, X. Jin, C. Cheng, Y. Li, K. Li. *Spectrochim. Acta, Part A*, **78**, 1278 (2011).
[27] S.J. Lau, T.P.A. Kruck, B. Sarkar. *J. Biol. Chem.*, **249**, 5878 (1974).
[28] C. Tanford. *J. Am. Chem. Soc.*, **74**, 211 (1952).
[29] H.A. Saroof, H.J. Mark. *J. Am. Chem. Soc.*, **75**, 1420 (1953).
[30] M.C. Beinfield, D.A. Bryce, D. Kochavy, A. Martonosi. *J. Biol. Chem.*, **250**, 6282 (1975).
[31] B.K. Jin, L.P. Lu. *Chin. Chem. Lett.*, **12**, 989 (2001).
[32] N.S. Quiming, R.B. Vergel, M.G. Nicolas, J.A. Villanueva. *J. Health Sci.*, **51**, 8 (2005).
[33] T. Peter. *Adv. Protein Chem.*, **37**, 161 (1985).
[34] M. Asadi, A.K. Bordbar, E. Safaei, J. Ghasami. *J. Mol. Struct.*, **705**, 41 (2004).
[35] M. Asadi, E. Safaei, B. Ranjbar, L. Hasani. *New J. Chem.*, **28**, 1227 (2004).
[36] M. Asadi. *J. Mol. Struct.*, **754**, 116 (2005).
[37] A. Bordbar, H. Dezhampanah, M. Asadi, E. Safaei, N. Sohrabi, Y. Khodadost. *J. Porphyrins Phthalocyanines*, **11**, 556 (2007).
[38] P. Kalck, F. Monteil. *Adv. Organomet. Chem.*, **34**, 219 (1992).
[39] P.T. Anastas, J.C. Warner. *Green Chemistry: Theory and Practice*, Oxford University Press, Inc., New York (1998).
[40] F. Moreno, M. Cortijo, J. González-Jiménez. *Photochem. Photobiol.*, **70**, 695 (1999).
[41] H. Weil, K. Brimmer. *Ber. Dtsch. Chem. Ges.*, **55B**, 301 (1922).
[42] E.A. Brustein, N.S. Vedenkina, M.N. Irkova. *Photochem. Photobiol.*, **18**, 263 (1973).
[43] T. Mossman. *J. Immunol. Methods*, **65**, 55 (1983).
[44] R. Yousefi, S.K. Ardestani, A.A. Saboury, A. Kariminia, M. Zeinali, M. Amani. *J. Biochem. Mol. Biol.*, **38**, 407 (2005).
[45] A.B.P. Lever. *Inorganic Electronic Spectroscopy*, 2nd Edn, Elsevier, New York (1984).
[46] A. Khandar, B. Shaabani, F. Belaj, A. Bakhtiari. *Polyhedron*, **25**, 1893 (2006).
[47] Y.L. Zhang, W.J. Ruan, X.J. Zhao, H.G. Wang, Z.A. Zhu. *Polyhedron*, **20**, 1535 (2003).
[48] J.W. Leadbetter Jr. *J. Phys. Chem.*, **81**, 54 (1977).
[49] I. Cavaco, J. Costa Pessoa, D. Costa, M.T.L. Duarte, R.T. Henriques, P.M. Matias, R.D. Gillard. *J. Chem. Soc., Dalton Trans.*, 1989 (1996).
[50] G.B. Deacon, R.J. Phillips. *Coord. Chem. Rev.*, **33**, 227 (1980).
[51] K. Nakamoto. *Infrared and Raman Spectra of Inorganic and Coordination Compounds*, 3rd Edn, Wiley & Sons, New York (1978).
[52] J. Ribas, C. Diaz, R. Costa, Y. Journauv, C. Mathoniere, O. Kahn, A. Gleizes. *Inorg. Chem.*, **29**, 2042 (1990).
[53] N.T. Abdel-Ghani, O.E. Sherif. *Thermochim. Acta*, **156**, 69 (1989).
[54] J.R. Lakowicz. *Principles of Fluorescence Spectroscopy*, 3rd Edn, Plenum, New York (2006).
[55] W.R. Ware. *J. Phys. Chem.*, **66**, 455 (1962).
[56] S.S. Lehrer. *Biochemistry*, **10**, 3254 (1971).
[57] M. Alain, B. Michel, D. Michel. *J. Chem. Educ.*, **63**, 365 (1986).
[58] S. Hogelberg, K. Hult, R. Fuchs. *J. Appl. Toxicol.*, **9**, 91 (1989).
[59] A. Sulkowska. *J. Mol. Struct.*, **614**, 227 (2002).
[60] S.A. Sugio, S. Kashima, M. Mochizuki, M. Noda, K. Kobayashi. *Protein Eng.*, **12**, 439 (1999).
[61] D.T. Haynie. *Biological Thermodynamics*, Cambridge University Press, Cambridge (2001).
[62] P.D. Ross, S. Subramanian. *Biochemistry*, **20**, 3096 (1981).
[63] T. Förster, O. Sinanoglu. *Modern Quantum Chemistry*, Vol. 3, Academic Press, New York (1966).
[64] L. Cyril, J.K. Earl, W.M. Sperry. *Biochemists' Handbook*, E. & F.N. Spon, London (1961).
[65] B. Valeur, J.C. Brochon. *New Trends in Fluorescence Spectroscopy*, 6th Edn, p. 25, Springer Press, Berlin (1999).
[66] B. Valeur. *Molecular Fluorescence*, Wiley Press, New York (2001).
[67] J.N. Miller. *Proc. Anal. Div. Chem. Soc.*, **16**, 203 (1979).
[68] H.Y. Shrivastava, T.R. Kumar, N. Shanmugasundaram, M. Babu, B.U. Nair. *Biol. Med.*, **38**, 58 (2005).
[69] M. Shakir, M. Azam, M.F. Ullah, S.M. Hadi. *Photochem. Photobiol.*, **104**, 449 (2011).